Measurements of ion velocity and density in the plasma sheath

M. J. Goeckner,[a] J. Goree,[b] and T. E. Sheridan[c]
Department of Physics and Astronomy, The University of Iowa, Iowa City, Iowa 52242

(Received 3 June 1991; accepted 15 January 1992)

Using laser-induced fluorescence, the ion velocity and density inside a dc plasma sheath have been measured. A polished planar electrode, biased at -100 V, was aligned so that a laser beam struck it at normal incidence. Using this arrangement, the ion velocity component perpendicular to the electrode surface was measured. By detecting the fluorescence while scanning the laser frequency, a line shape was recorded that had two peaks, due to the Doppler shift from the incident and reflected beams. The separation of the peaks yielded an absolutely calibrated measure of the ion drift velocity, while the height of the peaks gave the ion density. As expected, in the sheath the measured ion density was lower and the velocity was higher than in this plasma. Using these measurements, it was confirmed that the ion flux is conserved in this sheath. The spatial profiles of ion velocity and density in the sheath were used to test a time-independent two-fluid theory, and good agreement was found. The data were also compared to Child's law, which showed good agreement near the electrode but predicted the density poorly, as expected, near the plasma–sheath boundary.

I. INTRODUCTION

A plasma sheath is the localized electric field that separates a plasma from a material boundary. It confines the more mobile species in the plasma and accelerates the less mobile species out of the plasma and toward the walls. For the typical case where the electrons are more mobile than the positively charged ions, the electric field in the sheath points toward the boundary.

Understanding sheaths is perhaps one of the oldest problems in plasma physics.[1] The basic problem of plasma flowing into a wall is important in many aspects of plasma physics. Because of this, many models have been developed to describe sheaths. They include, for example, the theory of Langmuir probes,[2] and models of divertor plates in tokamaks.[3] These models range from simple analytical expressions, such as Child's law,[4] to complex kinetic simulations.[5]

Models have been used to predict how different physical processes influence sheaths. For example, if the potential at the wall is made to vary in time then so will the electric field in the sheath.[6,7] Magnetic fields[8] and collisions[9] can also modify the sheath.

Based on his experimental work, Langmuir was one of the first to properly model plasma sheaths.[1] He tested the model by comparing the predicted sheath width to a visual measurement of the width of the dark space at the plasma–electrode boundary. This method is still used as an imprecise method of measuring the sheath width.

Since Langmuir's experiments, many other measurements have been reported, including several that involved *in situ* characterization of the interior of the sheath. Using an electron beam, Goldan[10] measured the electric field in a planar dc sheath. Using an emissive probe, Cho *et al.*[11] measured the potential in a dc sheath. Cho *et al.* also examined the temporal response of the sheath potential to steplike and radio-frequency changes in the bias applied to the electrode. Using laser-induced fluorescence (LIF), Gottscho *et al.*[12] measured the time-dependent ion density in a radio-frequency sheath. Using LIF, Gottscho and Mandich[13] measured the electric field in a radio-frequency sheath.

In this paper, we report LIF measurements of the ion drift velocity and density in a dc sheath. To our knowledge this is the first time LIF measurements of ion velocities in a dc plasma sheath have been reported. The advantages of the LIF technique are that it provides nonperturbing, *in situ*, and velocity-resolved measurements. LIF also allows full three-dimensional spatial resolution. This is in contrast to optical glow measurements, which are always chord averaged, and thus provide only two-dimensional spatial resolution.

We compare these measurements to the predictions of the simple two-fluid model of plasma sheaths reviewed in Sec. II. In Sec. III, we describe the experimental apparatus and the LIF diagnostic technique. In Sec. IV, we compare our experimental results to the predictions of the fluid theory and find excellent agreement. Finally, in Sec. V, we summarize our results.

II. TWO-FLUID SHEATH THEORY

Here, we review a widely used[14] time-independent model that predicts the potential in a planar plasma sheath ϕ as a function of position x. One end of the plasma is terminated by a perfectly absorbing wall held at a negative potential ϕ_w. Here, and throughout this paper, the subscript w will refer to the wall or electrode. (The terms wall and electrode are used interchangeably in this paper.) We choose the position of the wall to be $x = 0$ (see Fig. 1). Far from the wall there is a

[a] Present address: Engineering Research Center for Plasma Aided Manufacturing, Room 101, 1410 Johnson Drive, University of Wisconsin, Madison, Wisconsin 53706-1806.
[b] On temporary leave to: Max-Planck-Institut für Extraterrestrische Physik, 8046 Garching bei München, Germany.
[c] Present address: Department of Physics, West Virginia University, 209 Hodges Hall, Morgantown, West Virginia 26506-6023.

 0899-8221/92/061663-08$04.00

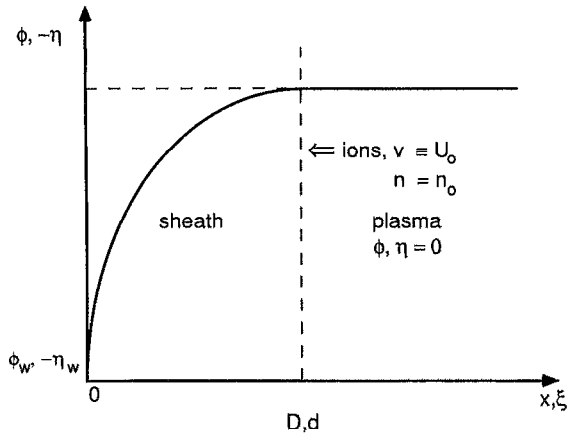

FIG. 1. Model system for the plasma sheath. The potential ϕ in the plasma sheath is sketched as a function of distance from the wall x. Ions enter the sheath as a monoenergetic beam with a velocity u_0. Dimensionless quantities are shown to the right of their dimensional counterparts. Note that the sign of the dimensionless potential, $\eta = -e\phi/kT_e$, is opposite that of ϕ.

field-free and neutral plasma where $\phi = 0$. The plasma consists of electrons and positive ions, which are both treated as fluids. The density of electrons n_e and ions n_i are both equal to n_0 in the plasma. At some point $x = D$, where D is the sheath thickness, there is a transition from the non-neutral sheath to the neutral plasma.

The governing equations of this model are based on a number of simplifying assumptions. First, it is assumed that the sheath parameters are time independent and as such we ignore any instabilities or waves in the sheath. Second, it is assumed that there is no impediment (e.g., a magnetic field parallel to the wall) to the free flow of electrons and ions to the wall. Third, the ion temperature is assumed to be negligible. Fourth, it is assumed that the sheath region is source-free and collisionless. Because the sheath is source free, the ion density obeys the equation of continuity, $n_i(x) = n_0 u_0/v(x)$. Here the ions enter the sheath with a velocity u_0, $v(x)$ is the velocity of the ions in the sheath region, and n_0 is the ion density at the sheath edge. Because the ions are assumed to be cold, they are a monoenergetic beam in the sheath. In this model, u_0 must be greater than the ion acoustic velocity c_s in order that ϕ decreases monotonically as we move toward the wall.[14] Because the sheath is collisionless, energy is conserved, and so $Mv^2 = Mu_0^2 + 2e\phi(x)$. Here, M is the ion mass and e is the charge. Combining the equations of continuity and conservation of energy we find that the ion density in the sheath is given by

$$n_i(x) = n_0(1 - 2e\phi/Mu_0^2)^{-1/2}, \tag{1}$$

while the the ion velocity is given by

$$v(x) = (u_0^2 - 2e\phi/M)^{1/2}. \tag{2}$$

Fifth, the electrons are assumed to be in thermal equilibrium. Accordingly, the electron density n_e obeys the Boltzmann relation

$$n_e = n_0 \exp(e\phi/kT_e). \tag{3}$$

Finally, the potential must satisfy Poisson's equation,

$$\frac{d^2\phi}{dx^2} = -\frac{e}{\epsilon_0}(n_i - n_e)$$

$$= -\frac{en_0}{\epsilon_0}\left[\left(1 - \frac{2e\phi}{Mu_0^2}\right)^{-1/2} - \exp\left(\frac{e\phi}{kT_e}\right)\right], \tag{4}$$

where ϵ_0 is the permittivity constant.

For convenience in solving these equations, they can be nondimensionalized by the following transformations:

$$\eta = -e\phi/kT_e, \tag{5a}$$

$$\xi = x/\lambda_D = x(n_0e^2/\epsilon_0 kT_e)^{1/2}, \tag{5b}$$

$$\mathcal{M} = \frac{u_0}{c_s} = \frac{u_0}{(kT_e/M)^{1/2}}. \tag{5c}$$

Here η is the dimensionless potential (note that the sign of η is opposite that of ϕ), ξ is distance from the electrode normalized by the Debye length, λ_D, and $\mathcal{M}$ is the Mach number. In dimensionless form, Poisson's equation [Eq. (4)] for the potential variation in the sheath is

$$\eta'' = (1 + 2\eta/\mathcal{M}^2)^{-1/2} - e^{-\eta}, \tag{6}$$

where η'' is the second derivative of η with respect to ξ. The first term on the right-hand side is the dimensionless ion density and the second term is the dimensionless electron density. The boundary conditions are $\eta(0) = \eta_w$ at the wall, and $\eta(\xi \to \infty) = 0$ in the plasma. Finally, the equations for continuity [Eq. (1)] and energy [Eq. (2)] are typically rewritten in dimensionless variables:

$$n_i(\xi)/n_0 = \mathcal{M}[\mathcal{M}^2 + 2\eta]^{-1/2}, \tag{7}$$

and

$$v(\xi)/c_s = [\mathcal{M}^2 + 2\eta]^{1/2}. \tag{8}$$

For this model the Bohm criterion[14] requires that $\mathcal{M} \geqslant 1$. Thus it is seen that the two-fluid model can be used to predict the ion density and velocity in the sheath [Eqs. (7) and (8)] provided the potential η can be determined from Poisson's equation.

There is no known closed-form analytic solution for Poisson's equation [Eq. (6)]. To determine η in the sheath, one must either use an approximate analytic solution or numerically solve Poisson's equation.

Child's law[4] is an approximate analytical solution of Poisson's equation that predicts the potential in the sheath. Satisfying the boundary conditions at the wall, $\eta(0) = \eta_w$, and at the plasma–sheath interface, $\eta(d) = 0$, and making the approximations reviewed in Ref. 15, a solution is

$$\eta(\xi) = [\tfrac{9}{4}(\mathcal{M}/\sqrt{2})]^{2/3}(d - \xi)^{4/3}, \quad \xi \leqslant d$$

$$= 0, \quad \xi > d. \tag{9}$$

The dimensionless sheath thickness d is given by

$$d = \tfrac{4}{3}(\eta_w^{3/4}/2^{3/4}\mathcal{M}^{1/2}). \tag{10}$$

This is the thickness of the region where the electron density is negligible. Equations (9) and (10) taken together are called Child's law. Child's law relates three quantities: the wall potential η_w, the sheath thickness d, and the Mach number $\mathcal{M}$. The mach number is related to the current density for ions entering the sheath. Hence, Child's law is often

used to determine the current density flowing into a sheath, $J_i \propto en_0 u_0 = en_0 c_s \mathscr{M}$, for given values[16] of η_w, and d, where d must be determined without using Eq. (10). It is well known[15] that Child's law is inaccurate for low potentials ($\eta_w < 10^4$) and near the sheath–plasma boundary ($\xi \approx d$).

One can also precisely solve Poisson's equation using numerical integration. Typically one would use an integration technique such as the Runge–Kutta method.[15] Numerical solutions are more accurate than Child's law.

Using the sheath potential profile $\eta(x)$ calculated from either a numerical solution of Poisson's equation [Eq. (6)] or Child's law [Eq. (9)], we can predict the ion velocity and density in the sheath. The velocity is predicted using the conservation of energy equation [Eq. (8)] while the density is found using the continuity equation [Eq. (7)]. We can compare these predictions to LIF measurements of the density and velocity.

III. APPARATUS

A. Multidipole device

The plasma chamber is sketched in Fig. 2. The vacuum vessel is divided into two sections, separated by a grid at ground potential. Thoriated-tungsten filaments are housed in a source chamber, which has water-cooled stainless-steel walls. The electrode is located downstream of the filaments in the larger 32 cm diam main chamber. The main chamber is made of aluminum that has been black anodized to reduce scattered light. It is equipped with Pyrex windows for making optical measurements.

The plasma was sustained by primary electrons emitted from the filaments, and it was confined by a multidipole magnetic field. The field was provided by 19 rows of ceramic magnets, arranged in a line cusp geometry.[17] In the center of the main chamber, where our LIF measurements were made, the magnetic field was measured to be less than 7 G. Our multidipole device is described in more detail in Ref. 18.

B. Electrode

The electrode assembly is sketched in Fig. 3. The electrode is a highly polished 50 mm diam stainless-steel disk. It is isolated from ground by a ceramic standoff. The back of the electrode is covered by an electrically floating aluminum shield. The electrode assembly is attached to a mirror mount that can be tilted on two axes, allowing us to adjust the electrode surface so that it is perpendicular to the laser beam.

A plasma sheath was formed by biasing the electrode negatively. A -100 V dc bias was supplied by an adjustable voltage-regulated power supply (Sorensen DCR 600-3B). (Like all voltages cited in this paper, this voltage is measured with respect to the grounded vacuum vessel.)

C. LIF diagnostic

LIF is widely used for characterizing plasma ions,[18–20] and works as follows. Laser light with frequency ν_L and wave vector $\mathbf{k}$ is fired into the plasma. The transition frequency of a stationary ion is ν_0, so that ions moving with the velocity $\mathbf{v}$ only absorb photons if the laser frequency satisfies the Doppler shift condition

$$2\pi\,\Delta\nu = 2\pi(\nu_L - \nu_0) = \mathbf{v}\cdot\mathbf{k} = v_\parallel k, \tag{11}$$

where $v_\parallel$ is the component of the ion velocity parallel to the direction of the laser beam. An ion that has absorbed a photon subsequently emits a fluorescence photon, as shown in Fig. 4. By scanning the laser frequency while measuring the

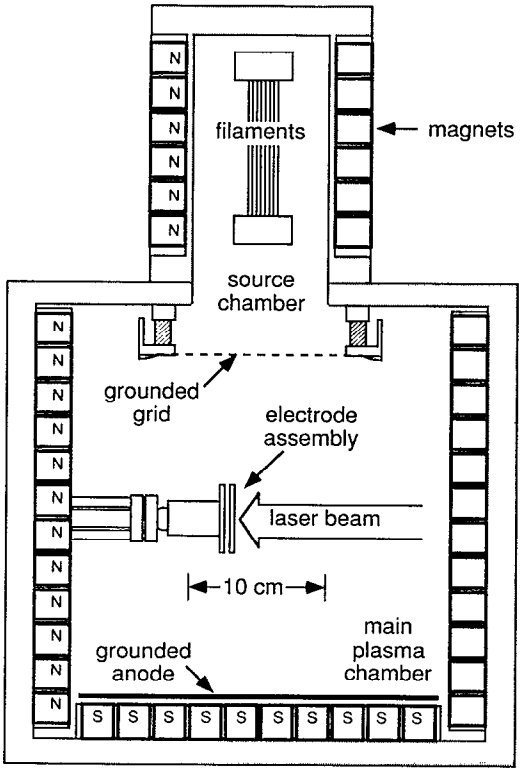

FIG. 2. Plasma chamber. Ceramic magnets arranged in a line-cusp geometry provide multidipole confinement of the plasma. A grounded grid divides the device into a source chamber, containing the filaments, and a larger main chamber. We used laser-induced fluorescence (LIF) to measure the ion density and drift velocity in the electrode sheath.

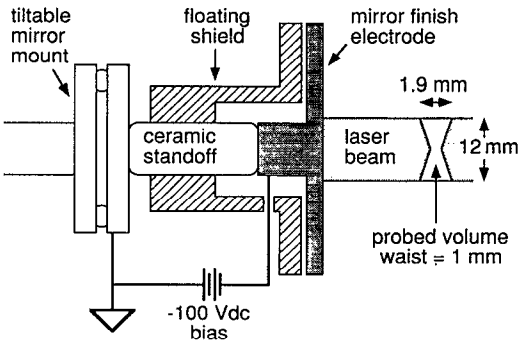

FIG. 3. Electrode assembly. This consists of a highly polished stainless-steel electrode, a ceramic standoff, and an electrically floating shield. It was mounted on a mirror mount that is adjustable on two axes, allowing us to align the laser beam for normal incidence. The shape of the probed volume is exaggerated to show details.

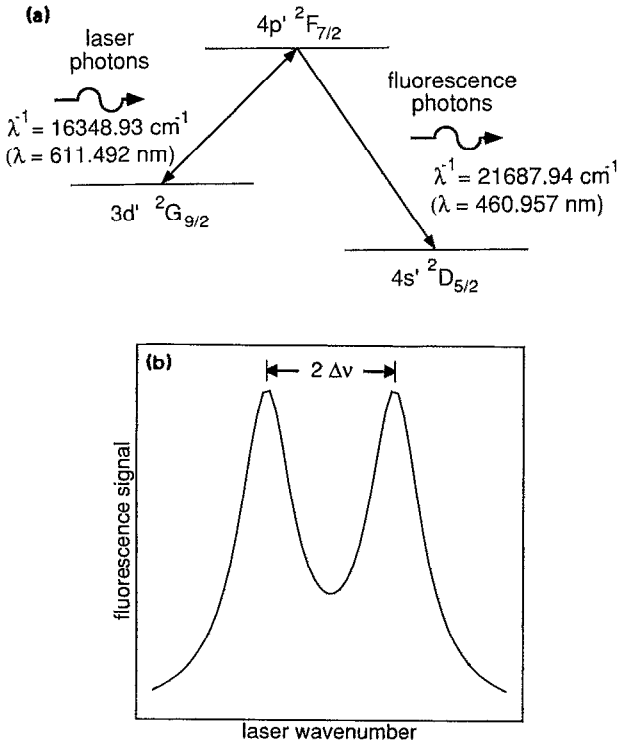

FIG. 4. LIF process. (a) Energy diagram. Argon ions are pumped from the $3d'^2G_{9/2}$ metastable state to $4p'^2F_{7/2}$. Photons produced by spontaneous decay from $4p'^2F_{7/2}$ to $4s'^2D_{5/2}$ constitute the fluorescence signal. The shape of the absorption spectral line is measured by scanning the laser through the $3d'^2G_{9/2} - 4p'^2F_{7/2}$ transition and recording the fluorescence signal. (b) Sketch of LIF line shape. The line shape has two peaks because of the separate Doppler shifts of the incident and reflected laser beams. Their separation 2 $\Delta\nu$ yields the ion drift velocity, using Eq. (11), while their heights provide a measure of the density.

resulting fluorescence intensity, the ion velocity component along the laser beam and the ion density can be determined. The ion velocity is found from Eq. (11), using the $\Delta\nu$ that results in the peak fluorescence signal. The density is proportional to the strength of the fluorescence at that peak.

We chose to probe the $3d'^2G_{9/2}$ metastable ion state because it is impossible to detect ground-state argon ions without using vacuum ultraviolet light. The atomic transitions are indicated in Fig. 4. The metastable state is probed using a laser frequency of 16 348.93 cm^{-1} (611.492 nm), and detecting fluorescence at 21 687.94 cm^{-1} (460.957 nm). Here, we report frequency in vacuum wave numbers (cm^{-1}) and wavelength in air (nm).

In another experiment, we found that this metastable state is a reliable indicator of the ion parameters.[18] Likewise in this experiment, the probed metastable ions should accurately represent the ions as a whole (most of which are in the ground state). All ions, independent of their excitation state, are subject to the same electrical forces. Since the lifetime[21] of the $3d'^2G_{9/2}$ state ($> 10\ \mu$sec) is much longer than the transit time through the sheath ($\approx 1\ \mu$sec), the ratio of the metastable-state ion density to the total ion density is the same everywhere in the sheath.

The electrode surface was made highly reflective so that both the incident and reflected laser beams would cause fluorescence. For ions moving toward the electrode, the incident beam is red shifted, while the reflected beam is blue shifted. Consequently, if the ions have a net drift velocity v_d, the fluorescence line shape will have peaks at two distinct frequencies ν_L. One peak is from the incident beam and the other from the reflected beam, as sketched in Fig. 4(b). Using Eq. (11), we see that these peaks will be separated by a frequency interval $2\Delta\nu = v_d k/\pi$. Thus the separation of the peaks is proportional to v_d, and provides an exact and absolute measure of the drift velocity.

The layout of the optical systems and the electrode is sketched in Fig. 5. We used a pulsed tunable dye laser (Lumonics HD-300), that was fired at a 10 Hz repetition rate and operated with a bandwidth of less than 0.09 cm^{-1} (2.7 GHz). A telescope was used to expand the beam so that it filled the desired volume. The telescope consisted of two 25 mm diam glass lenses, with focal lengths of -25 and $+125$ mm. A sample of the laser beam was diverted by a beamsplitter through an iodine cell. We compared the iodine fluorescence spectrum that we measured to the spectrum tabulated[22] in an atlas in order to calibrate the laser wavelength. To monitor the performance of the laser, a second sample of the beam was diverted to a laser power meter. The laser beam struck the electrode at normal incidence so that we measured the ion velocity component normal to the electrode surface. The beam was visually centered on the electrode to avoid the fringing effects of the sheath near the edge of the electrode.

The detection optics were positioned to view the sheath at an angle of 90° from the laser beam. A 150 mm focal length, 10 cm diam lens was used to collect the fluorescence from the plasma and focus it onto a 1 mm wide slit. This slit determined the chord that was viewed by the detection optics. The volume where this chord and the laser beam intersect defined the region of the plasma that was probed by the LIF apparatus. This volume was 1.9 mm long, 15 mm tall, and 12 mm wide, as sketched in Figs. 3 and 5. The elongated and thin shape of this "bowtie" volume was chosen to maximize the signal-to-noise ratio while preserving the spatial resolution in the direction of the laser beam. Ninety percent of the probed volume was within a 1.5 mm region along the laser beam's path. Thus we had an effective spatial resolution in the sheath of 1.5 mm. Directly behind the slit, a bandpass interference filter centered about 21 687.80 cm^{-1} (460.960 nm) was used to reduce extraneous light, particularly the white-hot glow from the filaments and any scattered laser light. The bandwidth of this filter, 24.04 cm^{-1}, is much wider than the Doppler shift of the fluorescence, < 1.75 cm^{-1}, and thus transmission of the fluorescence photons was independent of their Doppler shift. The fluorescence was detected by a photomultiplier tube (Thorn EMI 9659QB). The sensitivity of the detection optics was not calibrated.

The data acquisition scheme is also sketched in Fig. 5. The LIF signal from the plasma was amplified by 60 dB using a 300 MHz bandwidth amplifier. The LIF signals from the plasma and the iodine cell were recorded using a pair of

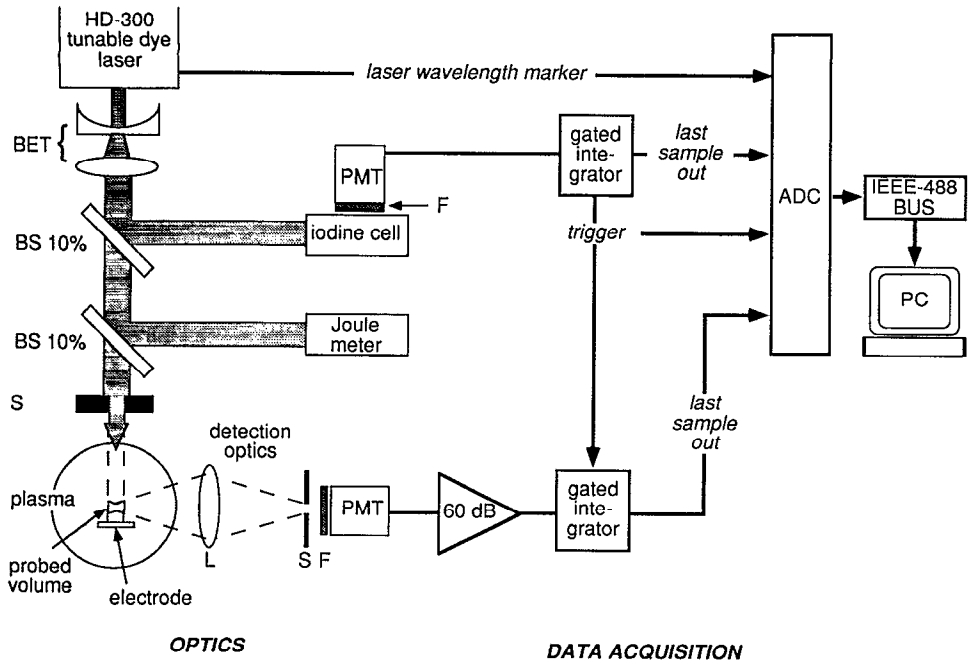

FIG. 5. Layout of the optical system and data acquisition for the LIF diagnostic. The optical equipment (not drawn to scale) includes a beam-expanding telescope (BET), a 100 mm diam, 150 mm focal-length lens (L), two beamsplitters (BS) with 10% reflectivities, two movable adjustable slits (S), two filters (F), and two photomultiplier tubes (PMT). We used a 24.04 cm^{-1} bandpass interference filter centered at 21 687.80 cm^{-1} for the plasma fluorescence and a red longpass filter for the iodine cell. The laser beam was reflected off of the electrode, back through the sheath. Adjusting the position of the slit S in the detection optics using a micrometer allowed us to select the distance x from the electrode.

boxcar integrators (Stanford Research SR250). Although it is common to use the analog averaging feature of boxcar integrators, we avoided this because it sacrifices the signal-to-noise ratio and skews the line shape. Instead, we numerically averaged the signal. To do this, the "last signal out" from the integrators was digitized by an analog-to-digital converter (Stanford Research SR250) after each laser shot. The signal was recorded on a computer and then averaged over many shots for each laser wavelength. Each shot was equally weighted. This procedure was repeated for a series of equally spaced laser wavelengths to measure the shift in the absorption spectral line and the intensity of the fluorescence. Further details of the data acquisition scheme are given in Ref. 18.

Several steps were taken to reduce noise levels and thus increase the signal-to-noise ratio. Scattered light (from all sources) was reduced by black anodizing the walls of the main chamber. The filaments were positioned so that they could not be directly seen by the detection optics. We added a baffle between the electrode and the 10 cm lens to block light scattered off the electrode, and used a baffle at the entrance window to suppress unwanted light scattered from that window. We thereby reduced noise levels until random fluorescence from the plasma was the largest source of noise.

These efforts to reduce the noise were crucial because the signal was very weak. There was on average less than one fluorescence photon detected per laser shot. The signal was this weak because of the low ion density and the small probed volume. (We chose to operate the plasma with a low ion density to provide a large Debye length and thus provide a large sheath width. The small probed volume was then chosen to give the desired spatial resolution.) To maximize the signal, we operated the laser with enough intensity to slightly saturate the transition.[23,24] Because of the low signal-to-noise ratio for a single shot, we averaged over multiple shots at the same laser wavelength. We found that 200 shots gave an adequate signal-to-noise ratio when the probed volume was far from the electrode, while closer to the electrode where the ion density is lower, as many as 1200 shots were required.

IV. EXPERIMENT

The discharge was almost identical to the one we reported in Ref. 18, where we used LIF to characterize the ions in a multidipole discharge. In that experiment, we used a different laser with a much narrower bandwidth, <0.013 cm^{-1}, so that we could resolve the shape of the ion velocity distribution. (Such narrow-band LIF measurements are often referred to as "sub-Doppler.") We found that the ions are always at room temperature, regardless of the gas pressure, discharge voltage, and discharge current. We also found that the density of the metastable ions is proportional to the density of the ions as a whole, provided the discharge voltage is at least -35 V.

The only difference between these two discharges is that here we inserted an electrode. The discharge for the present experiment had a neutral Ar pressure of 0.050 Pa (Ar calibrated), a constant discharge current of 0.10 A, and a discharge voltage of -40 V. The electrode was biased at -100 V, and drew a current of 0.189 mA from the plasma. This is $<2\%$ of the discharge current, indicating that the loss of plasma to the electrode was not a significant perturbation. Plasma parameters far from the electrode were determined using a cylindrical Langmuir probe with a diameter of 0.25 mm, and a length of 3.0 mm. Outside the plasma sheath the plasma potential was $+0.46$ V, the electron temperature was $T_e = 0.53$ eV, and the electron density was $n_e = 0.9 \times 10^{14}$ m^{-3}. Using these values, we calculate that the Debye length was $\lambda_D = 0.57$ mm. We were unable to measure plasma parameters in the sheath using the Lang-

muir probe. However, using LIF we were able to characterize the ion parameters in the sheath.

We used the LIF diagnostic to measure the ion drift velocity and relative density in the sheath and presheath at 13 different positions. The position x was selected by moving the slit in the detection optics with a micrometer. As the sheath width was ≈ 20 mm, the spatial resolution of 1.5 mm was adequate. The LIF measurements of v_d and n_i were made by scanning the laser through the 16 348.93 cm^{-1} (611.492 nm) excitation line[25] of the $3d'^2G_{9/2}$ metastable state of the argon ions,[21] and recording the intensity of the fluorescence[25] emitted at 21 687.94 cm^{-1} (460.957 nm). This scan covered a range of 3.5 cm^{-1} in steps of 0.05 cm^{-1}.

Since the transition was saturated and the laser bandwidth was wide, the detailed shape of the ion velocity distribution function could not be determined.[18,20] For this experiment, the minimum detectable split in the line shape occurred for a drift velocity of 2500 m/sec, which is much greater than the ion thermal velocity of 240 m/sec. LIF measurements such as these are called "broadband" rather than "sub-Doppler."

V. RESULTS AND DISCUSSION

A. Ion parameters

The LIF line shapes measured at 13 positions in the sheath and presheath are shown in Figs. 6 and 7. Note that close to the electrode the LIF signal is weak, indicating that the ion density is lower. At more than 19 mm from the electrode, we observe only a single peak, indicating that the ion drift velocity is below the resolution (2500 m/sec) of the apparatus. Closer to the electrode, we observe the expected double peaks. The separation of the peaks increases as one moves closer to the sheath, indicating that the ions are being accelerated to higher velocities near the electrode.

To determine the ion density and velocity accurately from the measured line shapes, we fit the data to a model line shape using a nonlinear least-squares routine. For the model, we chose to use the sum of two Lorentzians displaced from one another by a Doppler shift $2\Delta\nu$, and this fit the data well. The two Lorentzians were constrained to have the same height and width, but with opposite Doppler shifts, since the incident and reflected peaks should be symmetric. The separation of these peaks was used to determine the ion velocity using Eq. (11). The height of a single Lorentzian was assumed to be proportional to the ion density. The Doppler shift provides a very reliable and absolutely calibrated measure of the velocity. Error bars in the velocity measurement arise predominately because of a limited signal-to-noise ratio. Measurements of the density on the other hand are not as precise as the velocity measurements. This is because of various geometric and atomic physics factors. Finally, we note that the measurements of the density are not absolutely calibrated, but are reported in arbitrary units.

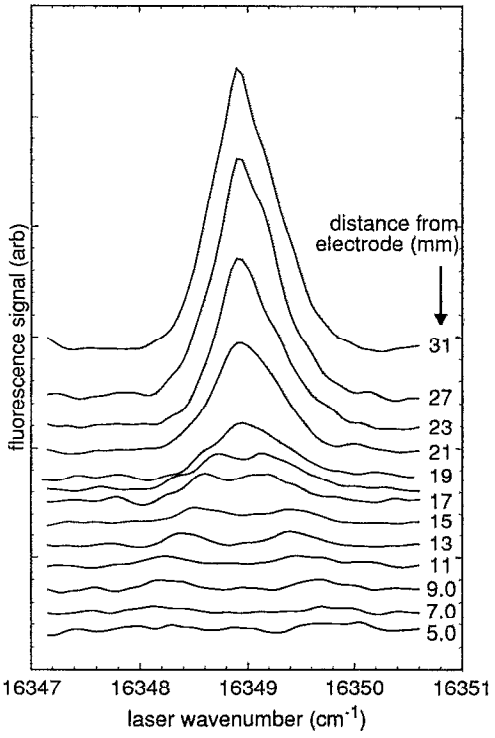

FIG. 6. Fluorescence line shape as a function of distance to electrode. The height of the line shape indicates the relative density of the ions. Note that near the electrode the density is less. These LIF measurements were made in an argon plasma with pressure $P = 0.050$ Pa, discharge voltage $V_{dis} = -40.0$ V, current $I_{dis} = 0.1$ A, and electrode bias $V_{electrode} = -100.0$ V. In this figure and Fig. 7, the data have been smoothed with a Gaussian filter to aid the eye.

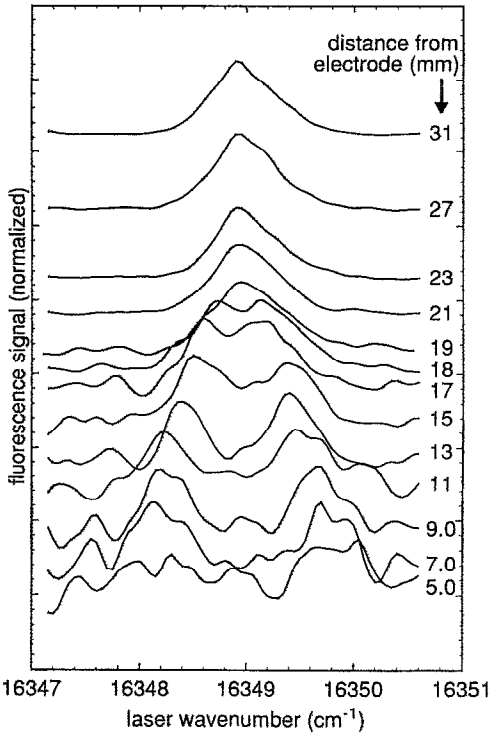

FIG. 7. Line shapes from Fig. 6, normalized to equal height. In the sheath the line shape has two peaks, one each for the incident and reflected beams. Larger separations in the peaks indicate larger ion velocities. Note that near the electrode the peaks are widely separated, indicating a large drift velocity.

The experimental ion densities, velocities, and fluxes (n_i v_d) are presented in Fig. 8. They are presented as functions of x, the distance from the electrode. These spatial profiles are the main results of this paper. As expected, the ion density decays precipitously in the sheath, the velocity increases, and the ion flux is conserved.

Using conservation of energy, Eq. (2), we computed the potential $\phi(x)$ from the measured ion velocity. As expected, the results shown in Fig. 8(d) reveal that in the sheath the potential monotonically increases with distance from the electrode, and in the presheath it is constant.

B. Comparison to fluid theory

As discussed in Sec. II, the two-fluid theory provides a simple model of plasma sheaths. The theory centers on Poisson's equation, Eq. (6), which can be solved either numerically or with an approximate analytic equation such as Child's law, Eq. (9).

We have endeavored to perform our experiment under conditions similar to the conditions assumed in the theory. First, the ion temperature was much less than the electron temperature ($T_i/T_e \ll 1$). Thus the approximation of cold ions in the theory is reasonable for this discharge. Second, in the sheath neither the ions nor the electrons are magnetized. This can be confirmed by noting that the ratio of the ion Larmor radius to the Debye length is greater than 256 and the ratio of the electron Larmor radius to the Debye length is greater than 5. Additionally, the geometry of the experiment indicates that the magnetic field is not parallel to the electrode's surface. Thus electrons trapped on magnetic field

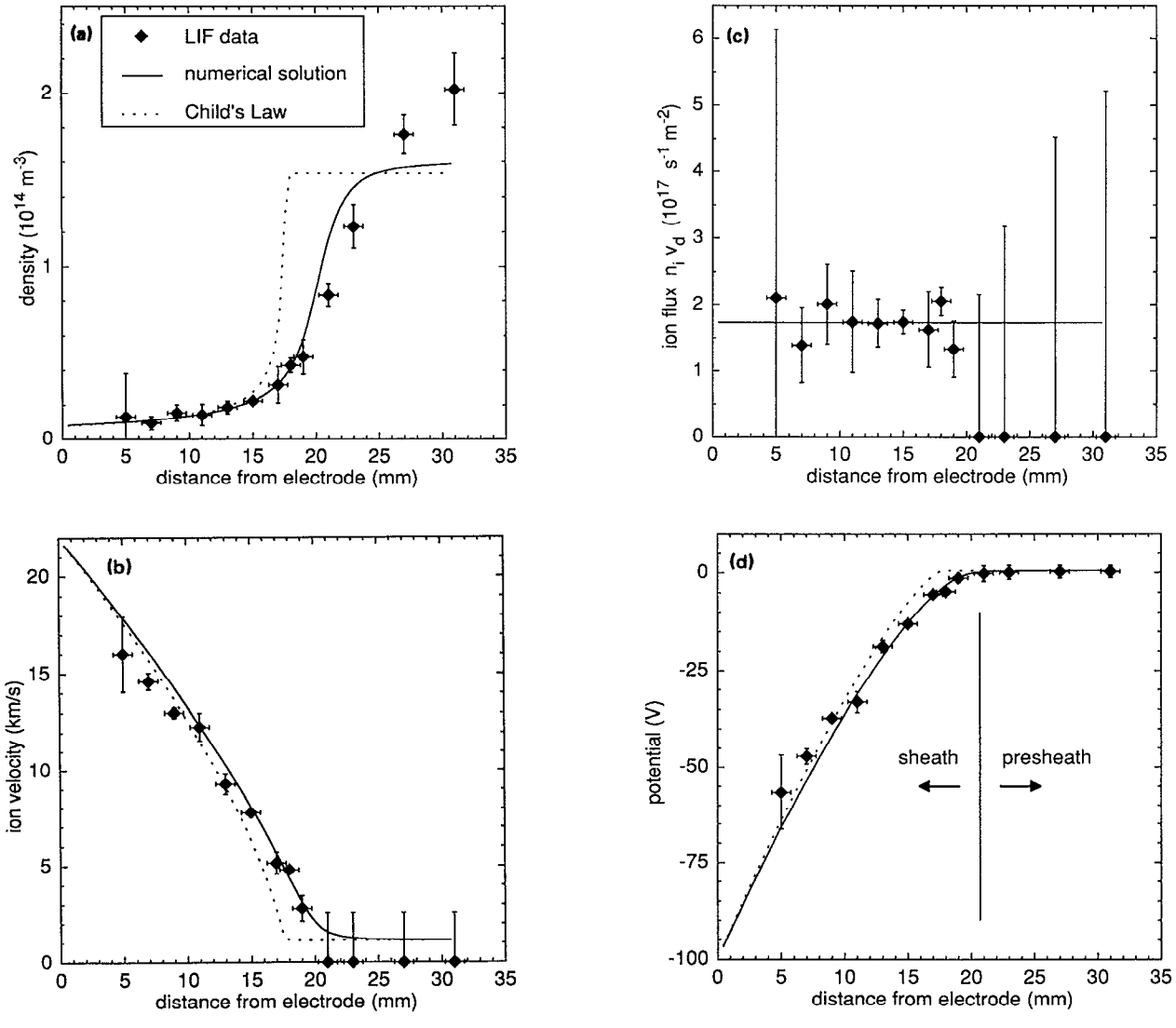

FIG. 8. LIF measurements compared to the numerical and Child's law solutions of the two-fluid sheath model. (a) The ion density n_i profile compared to the theoretical prediction. Because the densities from the LIF measurements and the numerical solution are in arbitrary units, we have scaled them to match at 18 mm from the electrode using the density found in Sec. V B. (b) The ion velocity v_d profile compared to the theoretical prediction. Because the Doppler shift technique provides an absolutely calibrated measure of the velocity, these data are the most accurate. (c) The ion flux n_i v_d compared to the theoretical prediction that it is a constant, i.e., that the ion flux is conserved. (d) The potential computed from the experimental velocity in (b) using energy conservation, Eq. (8), compared to the theoretical predictions. Here, as in (a) and (b), the numerical solution provides a better fit to the experimental data.

lines can easily enter the sheath with effectively no impediment. Third, the ions are noncollisional in the sheath. This is true because the Coulomb and ion–neutral collision mean-free paths (40 and 20 cm, respectively) are much longer than the sheath width ($\approx$2 cm). Fourth, the electrode was planar. Fifth, the discharge was dc. One difference between our experiment and the assumptions of the model is the presence of fast primary electrons in the experiment.[26] Our discharge was sustained by primary electrons emitted from the filaments. These primary electrons are more energetic than the bulk of the electrons, but are much less numerous. They are not accounted for in the theory described in Sec. II.

There is good agreement between the experimental results and the theoretical predictions, particularly the exact numerical solution. In Figs. 8(a) and 8(b) the measured ion densities and velocities are compared to the predictions of the exact numerical solution of the two-fluid model. To prepare the exact solution shown in Fig. 8, we solved the nondimensionalized Poisson equation [Eq. (6)] using a fourth-order Runge–Kutta integration technique.[15] We then sought the best possible fit by allowing T_e and λ_d to be free parameters. Using an eyeball fit, we found the best fit for both the exact solution and Child's law with $T_e = 0.53$ eV and $\lambda_d = 0.46$ mm. These values correspond to a density in the plasma of $n_0 = 1.1\times10^{14}\,\mathrm{m}^{-3}$. We have used this value of the density to calibrate all of the experimentally measured densities in Figs. 8(a) and 8(c). These fit parameters agree well with the Langmuir probe results: $T_e = 0.53$ eV, $n_0 = 0.9\times10^{14}\,\mathrm{m}^{-3}$, and $\lambda_d = 0.57$ mm. Thus it is seen that the two-fluid theory provides an accurate model of dc sheaths.

Child's law, on the other hand, does not predict the experimental results as well as the exact numerical solution. This is especially true for the density near the plasma–sheath boundary. This is because, as is well known,[15] Child's law is inaccurate near the plasma–sheath boundary.

As a final check of two-fluid theory, we tested the assumption that ion flux is conserved in the sheath. This assumption is embodied in the equation of continuity, $n_i(x)\,v(x) = n_0 u_0$. The experimental data shown in Fig. 8(c) confirms that flux is indeed conserved.

VI. SUMMARY

Using LIF, we measured the ion velocity and density in a dc plasma sheath. To measure these parameters, the laser beam was aimed at a polished electrode. By detecting the fluorescence while scanning the laser frequency, we measured a line shape with two peaks, one from the incident beam and one from the reflected beam. The separation of the peaks yielded an absolutely calibrated measure of the ion drift velocity, while the height of the peaks yielded the ion density. As expected, it was found that the ion density decreased and the velocity increased as one neared the electrode. Good agreement between the experiment and the time-independent two-fluid theory is found for the spatial profiles of the velocity and density in the sheath. We also compared the data to Child's law, which showed good agreement near the electrode but predicted the density poorly, as expected, near the plasma–sheath boundary. Finally, as a check on the two-fluid model, we computed the ion flux from our experimental data and confirmed that the ions obey the time-independent continuity equation in the sheath.

ACKNOWLEDGMENT

This work was funded by a grant from the Iowa Department of Economic Development.

[1] *The Collected Works of Irving Langmuir, Vol. 4*, edited by C. Guy Suits (Pergamon, New York, 1961), pp. 1–98.
[2] F. F. Chen, in *Plasma Diagnostic Techniques*, edited by R. H. Huddlestone and S. L. Leonard (Academic, New York, 1965), pp. 113–200.
[3] A. H. Boozer, Phys. Fluids **19**, 1210 (1976).
[4] C. D. Child, Phys. Rev. **32**, 492 (1911).
[5] R. J. Procassini, C. K. Birdsall, and E. C. Morse, Phys. Fluids B **2**, 3191 (1990).
[6] M. A. Lieberman, IEEE Trans. Plasma Sci. **PS-16**, 638 (1988).
[7] M. A. Lieberman, J. Appl. Phys. **65**, 4186 (1989).
[8] P. L. Auer, Phys. Fluids **26**, 1212 (1981).
[9] T. E. Sheridan and J. Goree, Phys. Fluids B **3**, 2796 (1991).
[10] P. D. Goldan, Phys. Fluids **13**, 1055 (1970).
[11] M. H. Cho, N. Hershkowitz, and T. Intrator, J. Vac. Sci. Technol. A **6**, 2978 (1988).
[12] R. A. Gottscho, R. H. Burton, D. L. Flamm, V. M. Donnelly, and G. P. Davis, J. Appl. Phys. **55**, 2707 (1984).
[13] R. A. Gottscho and M. L. Mandich, J. Vac. Sci. Technol. A **3**, 617 (1985).
[14] F. F. Chen, *Introduction to Plasma Physics* (Plenum, New York, 1974), pp. 244–249.
[15] T. E. Sheridan and J. Goree, IEEE Trans. Plasma Sci. **PS-17**, 884 (1989).
[16] P. Martin and G. Donoso, Phys. Fluids B **1**, 247 (1989).
[17] K. N. Leung, T. K. Samec, and A. Lamm, Phys. Lett. A **51**, 490 (1975).
[18] M. J. Goeckner, J. Goree, and T. E. Sheridan, Phys. Fluids B **3**, 2913 (1991).
[19] R. A. Stern and J. A. Johnson, III, Phys. Rev. Lett. **34**, 1548 (1975).
[20] M. J. Goeckner, J. Goree, and T. E. Sheridan, J. Vac. Sci. Technol. A **8**, 3920 (1990).
[21] P. Varga, W. Hofer, and H. Winter, J. Phys. B **14**, 1341 (1981).
[22] S. Gerstenkorn and P. Luc, *Atlas du Spectre d'Absorption de la Molecule d'Iode* (CNRS Editions, Paris, 1976).
[23] M. J. Goeckner and J. Goree, J. Vac. Sci. Technol. A **7**, 977 (1989).
[24] M. J. Goeckner, J. Goree, and T. E. Sheridan, in *Proceedings of the Fourth International Laser Science Conference*, Atlanta, 2–6 October 1988 (American Institute of Physics, New York, 1989), pp. 761–766.
[25] S. Bashkin and J. A. Stoner, Jr., *Atomic Energy Level & Grotrian Diagrams* (North-Holland, New York, 1978), Vol. 2, pp. 192–229.
[26] Because the primary electrons leave the chamber faster than the bulk of the plasma, we attempted to use LIF to characterize the sheath in the afterglow of a pulsed plasma. However, we found that the signal decayed too rapidly to make this practical.